JOURNAL OF PROPULSION AND POWER
Vol. 20, No. 6, November–December 2004

Zero-Dimensional Model for Preliminary Design of Ablative Pulsed Plasma Teflon® Thrusters

Claude M. Brito*
92100 Boulogne, France
Sergio A. Elaskar†
Instituto Universitario Aeronaútico, 5022 Córdoba, Argentina
Héctor H. Brito‡
Instituto Universitario Aeronáutico, 5022 Córdoba, Argentina
and
Nora R. Paoletti§
Universidad Nacional de Córdoba, 5000 Córdoba, Argentina

A new procedure to estimate the ablated mass in ablative pulsed plasma thrusters (APPTs) is presented throughout this paper. The procedure is based on considering the energy balance as related to the generation and transport of the current pulse, arc formation, heat dissipation by joule effect, and the plasma acceleration. This new balance equation is written in terms of the ablated mass of Teflon® as a function of the main electric and geometric parameters. The introduction of an ideal arc thickness in the descriptive equations allows the buildup of a simplified model well suited for the prediction of performances and for preliminary design purposes. The resulting analytical model shows the ability to reproduce trends and behaviors having already been observed theoretically as well as experimentally by other authors. On the quantitative side, this new model allows for improved performance predictions as compared with semi-empirical models. Comparison of the theoretical results obtained by means of this model for the impulse bit, with the experimental figures corresponding to five APPTs, results in an average relative error around 20%.

Nomenclature

A	=	cross section of the acceleration chamber, m^2
A_p	=	Teflon® exposed area, m^2
A_{rad}	=	arc radiation area, m^2
C	=	capacity of the capacitor bank, F
$c_{p,v}$	=	specific heats, J/kg K
E	=	energy, J
e	=	thickness of the parallel plate electrode, m
e_{gas}	=	ablation and sublimation energy of Teflon®, J/kg
h	=	enthalpy, J/kg
h_e	=	distances among parallel plate electrodes, m
h_0	=	total enthalpy, J/kg
I	=	impulse bit, Ns
I_b	=	electric current intensity, A
K	=	kinetic energy, J
k	=	Boltzmann constant, J/K
L	=	inductance, H
L'	=	inductance gradient along plasma flow direction, H/m
l	=	length of the subsonic cavity, m
l_e	=	electrode length, m
M	=	atomic mass of neutral products, kg
m	=	ablated mass per pulse, kg
p	=	neutral gas mean pressure, Pa
R	=	universal constant of gases, J/kg K
R_{ESR}	=	capacitors resistance, Ω
R_{PPT}	=	plasma + electrodes resistance, Ω
R_{tot}	=	total resistance, Ω
R_{trans}	=	transmission lines resistance, Ω
R_Ω	=	ohmic resistance, Ω
r	=	neutral gas constant, J/kg K
r	=	coaxial electrodes radius, m
T	=	plasma mean temperature, K
t_a	=	plasma-pulsed-thruster action time, s
t_{LRC}	=	current pulse period, s
t_m	=	time at maximum current intensity, s
t_{rad}	=	action time of arc radiation, s
U	=	internal energy, J
V	=	voltage, V
v	=	velocity, m/s
w	=	width of the parallel plate electrode, m
Z	=	ionization number
α_A	=	exposed Teflon area/radiation exposed area
α_i	=	ratio between the ionized mass and the total ablated mass
γ	=	adiabatic exponent
δ	=	ideal arc thickness, m
$(\varepsilon_i)_Z$	=	specific ionization enthalpy, eV/Kg
η	=	efficiency
η_L	=	Lorentz gas resistivity, Ω m
η_Ω	=	plasma ohmic resistivity, Ω m
σ	=	Stephan–Boltzmann constant, W/m^{2}K^4
ω	=	LRC circuit resonance angular frequency, s^{-1}

Subscripts

acc	=	inside the accelerator
an	=	annular (for coaxial electrodes)
arc	=	inside the arc
c	=	central (for coaxial electrodes)

Received 16 April 2003; revision received 29 March 2004; accepted for publication 4 May 2004.

*Master in Aeronautical and Space Techniques (Sup'Aéro), Consultant, 5, cours des Long Prés.

†Doctor in Engineering Sciences, Head, Department of Aeronautics, Av. Vélez Sarsfield 1601; currently CONICET and Universidad Nacional de Córdoba, 5000 Córdoba, Argentina. Member AIAA.

‡Ingénieur Civil de l'Aéronautique (Sup'Aéro), Project Manager, Applied Research Center, Ruta 20 km 5.5. Senior Member AIAA.

§Master in Propulsion Systems (Sup'Aéro), Ph.D. Student, Av. Vélez Sarsfield 1601.

cat	=	cathode
ESR	=	equivalent resistance of the capacitor bank
em	=	electromagnetic
et	=	gasdynamics
ext	=	outside the plasma flow
fi	=	ionized frozen flow
fn	=	neutral mass frozen flow
i	=	related to ions
joule	=	Joule effect
n	=	related to neutral masses
PPT	=	related to the ideal ablative plasma pulsed thruster
rad	=	radiant
sh	=	inside the sheaths
trans	=	related to transmission lines
0	=	energy or voltage in the capacitor bank

Introduction

THE ablative plasma pulsed thrusters (APPT) are very convenient propulsion devices for applications on orbit maintenance, attitude control, and formation flying, because of their ability to produce small impulse bits and high specific impulses with high reliability.[1] The use of Teflon® (as propellant) gives the additional benefit of a compact design and safety of operation.[2]

The APPT shown in Fig. 1a starts its operation cycle whenever the power processing unit gets power from the satellite bus, loading the capacitor bank up to the operating voltage V_0. The Teflon bar is fed between a couple of electrodes, which share the capacitors voltage V_0. An ignition spark plug, which consists of a semiconductor layer ring surrounded by another couple of electrodes, is fired through a small discharge. This has the effect of increasing the electric conductivity in the acceleration chamber so as to allow the discharge of the capacitors through arcing between the main electrodes, therefore liberating the stored electric energy and producing the ablation of a Teflon layer.

The electric current flows from the capacitors through the acceleration electrodes and the arc; a current loop builds up, and a magnetic field is accordingly generated. A microscopically thin layer of the Teflon exposed surface is removed by ablation, then partially ionized, and, finally, accelerated by means of the Lorentz force arising from the arc and the induced magnetic field interaction. An important fraction of the ablated mass is not ionized (remains neutral) but, because of the high temperatures present in the arc, is also accelerated by gasdynamics effects. Therefore, the ablated mass is accelerated by the combined effects of gasdynamics and electromagnetic forces. After the capacitors are fully discharged, the cycle repeats, and a pulsed operating regime can thus be achieved.

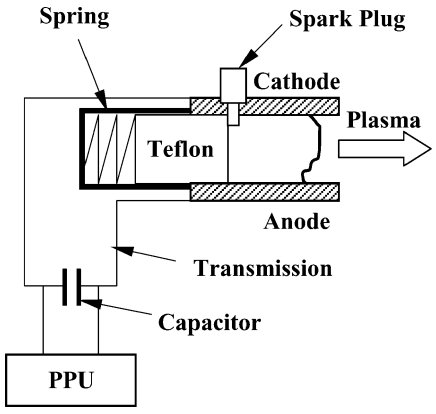

Fig. 1a Outline of the APPT.

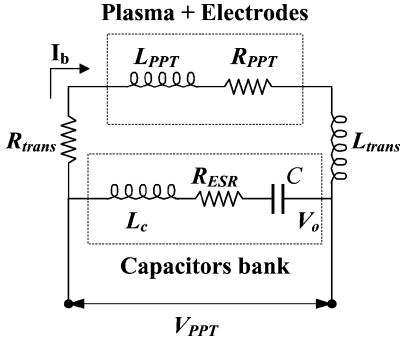

Fig. 1b Idealized electronics of the APPT.

The final detailed design of an APPT device requires the use of complex computer codes, which must be able to simulate the coupling between electric, geometric, gasdynamics, magnetogasdynamics parameters, and the unsteady mechanism of arc formation.[3,4] Some models of the electric discharge are based on the solution of time-dependent equations systems that take in consideration the energy balance, the Teflon ablation, and the mass conservation. These models are complete enough for the functional description of the APPT, but they are often entirely developed for a particular geometric configuration, and the extension of their use and results to other geometries is not straighforward.[5]

Empirical models have also been proposed based on ablation functions for different geometries. These models relies on curve fitting of experimental data, and their accuracy is restricted to APPTs working under similar experimental conditions.[6–8]

The aim of this paper is to present a new theoretical approach relating the ablated mass to the main electric and geometric parameters. A descriptive equation is obtained by considering the energy balance involved in the generation of the current pulse, its transport to and from the electrodes, the arc generation, heat dissipation by Joule effect, and the plasma acceleration. The formal introduction of an ideal arc thickness in the descriptive equation of the forementioned processes allowed the definition of a simplified model, which may be used for the APPT preliminary design.

Analytical Model for the Prediction of the Ablated Mass

In this section the new theoretical model for the calculation of the ablated mass and the impulse bit is derived. The section is divided into two subsections: The first one presents the assumptions involved in the derivation of the various analytical relationships. The second subsection embodies the mathematical derivation of the new descriptive equation.

General Assumptions

The following assumptions are made to obtain a simple analytical model:

1) The APPT behavior is modeled by means of a zero-dimensional analysis; it is then an algebraic model.

2) The energy balance starts at the capacitor bank because the discharge time is basically governed by this device. Besides, the capacitor bank represents the first location where energy losses become significant.[9]

3) The acceleration chamber, the electrodes, and the plasma are viewed as components of a resistive, capacitive, inductive (RLC) electric circuit with non-time-dependent parameters, Fig. 1b. This idealization permits the consideration of the plasma as a movable conductor bearing resistance and inductance,[10] allowing in turn the definition of the electromagnetic impulse associated with the acceleration of the ionic "cloud."[11]

4) Although the emissivity of the plasma is unknown, because of simplicity, its value is fixed to be one (blackbody radiator), as considered in Ref. 11.

5) According to Ref. 11, the necessary specific energy for the ablation of Teflon is 1.5×10^6 J/kg, which includes the energy for the breakdown of Teflon polymer chains and the specific energy necessary for the transition to the gaseous phase.

6) The plasma (formed by C and F particles existing in neutral, simple, and doubly ionized states) is supposed to be confined within a volume at uniform temperature.[5,11]

7) Neutral masses expand as a perfect gas in a subsonic cavity. The volume of this cavity is closely equal to the volume of the acceleration chamber. The highest gas velocity will then be the velocity of sound as calculated by using gasdynamics theory.[11]

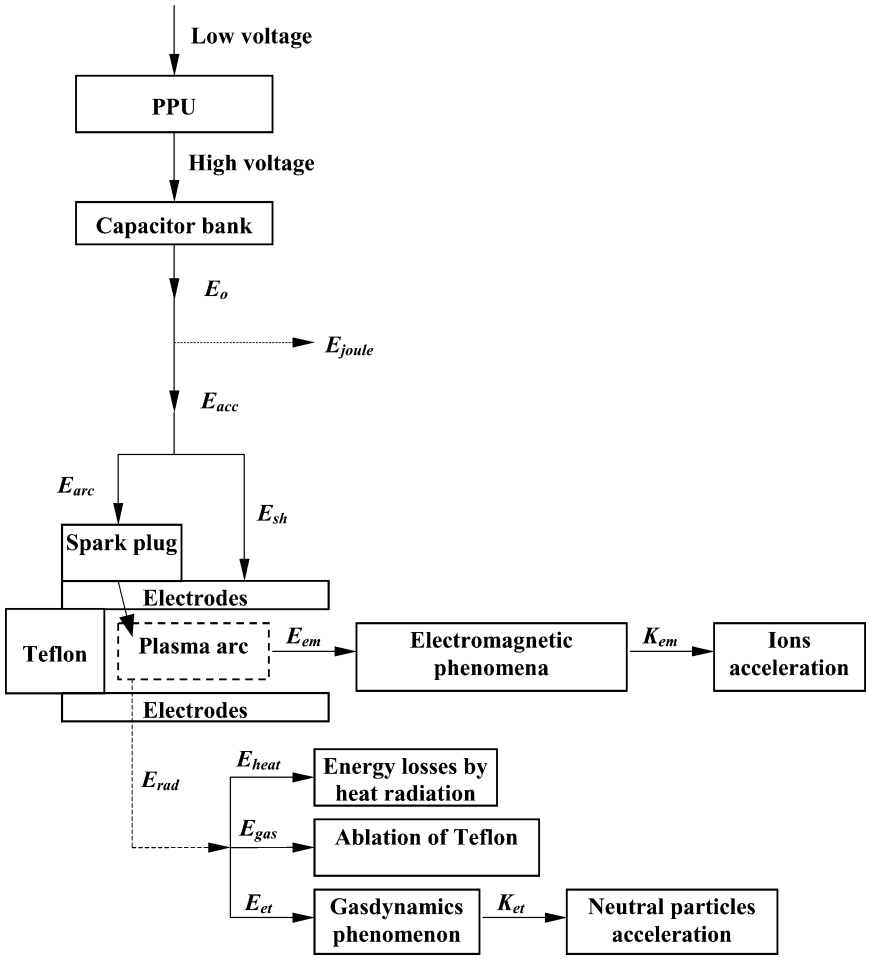

Fig. 2 Energy balance of an APPT.

8) The ionic and neutral masses are supposed to be $m_i = (0.1 \pm 0.05)m$ and $m_n = (0.9 \pm 0.05)m$, respectively. However, Spanjers et al.[12] found experimental values for m_i/m rising up to 0.25.

Energy Distribution Inside an APPT

The energies involved in an APPT module are shown in Fig. 2. The following energy balance can be written:

$$E_0 = E_{\text{joule}} + E_{\text{sh}} + E_{\text{heat}} + E_{\text{gas}} + E_{\text{em}} + E_{\text{et}} \tag{1}$$

where E_0 is the energy stored in the capacitors, E_{joule} is the energy loss by Joule effect in the transmission lines, E_{sh} is the energy loss at the potential sheaths, E_{heat} represents the radiation loss from the plasma, E_{gas} is the energy required to ablate and sublimate the Teflon into the gas phase comprising the depolymerization and the phase transition, E_{em} is the electromagnetic energy in the plasma jet (caused by ionized particles), and E_{et} is the energy related to the gasdynamics effects (caused by neutral particles). The three first terms of the right-hand side (RHS) represent energy losses, and so they do not contribute to the impulse. However, the last three terms of the RHS are ablated mass dependent. Therefore, the energies involved in Eq. (1) can be written in terms of the efficiencies and/or ablated mass (except E_0). It is thus convenient to express the energy balance in terms of the ablated mass. As a result, an equation will be obtained, which couples the ablated mass, the efficiencies related to the energy stored in the capacitor bank, the current transport by imperfect wires, the voltage losses in the potential sheaths, the heat dissipation in the arc, and the velocity losses in the plasma as a result of collisions between ions and neutral atoms.

Energy Dissipation by Joule Effect in the Wires

The energy dissipated in the wires can be expressed as a function of the efficiency η_{trans}. This coefficient represents the percentage of energy liberated by the capacitors that effectively reaches the accelerator

$$E_{\text{joule}} = (1 - \eta_{\text{trans}})E_0 \tag{2}$$

Because of assumption 3, the total resistance can be expressed as a function of the resistance of the transmission lines, the capacitors resistance, and the plasma resistance:

$$R_{\text{tot}} = R_{\text{trans}} + R_{\text{ESR}} + R_{\text{PPT}}$$

where

$$R_{\text{PPT}} = f(\delta)$$

By using the following expressions

$$E_{\text{acc}} = R_{\text{PPT}} \int_0^{t_a} I_b^2 \, \mathrm{d}t, \qquad E_0 = R_{\text{tot}} \int_0^{t_a} I_b^2 \, \mathrm{d}t$$

the efficiency η_{trans} becomes

$$\eta_{\text{trans}} = E_{\text{acc}}/E_0 = R_{\text{PPT}}/R_{\text{tot}} \tag{3}$$

where E_{acc} is the energy input to the acceleration chamber.

Energy at the Potential Sheaths

If η_{sh} represents the fraction of E_{acc} that is effectively used for the arc generation, the energy losses at the electrodes can be written as

$$E_{\text{sh}} = (1 - \eta_{\text{sh}})\eta_{\text{trans}} E_0 \tag{4}$$

The voltage between electrodes V_{PPT} is (see Figs. 1 and 3):

$$V_{\text{PPT}} = V_{\text{sh}} + I_{\text{b}} R_{\text{PPT}} + L_{\text{PPT}} \frac{\mathrm{d}I_b}{\mathrm{d}t}$$

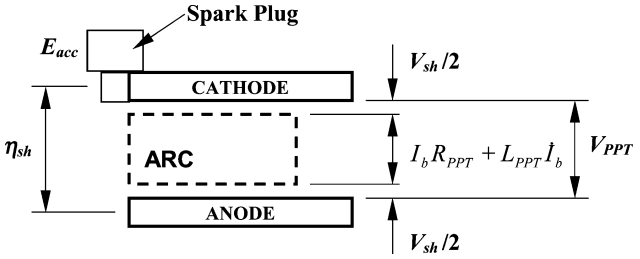

Fig. 3 The η_{sh} determination in function of the voltage losses at the potential sheaths.

the efficiency $\eta_{\rm sh}$ can then be written as a function of the power developed by the system electrodes, sheaths, and plasma, together with the power losses at the sheaths

$$\eta_{\rm sh} = \frac{E_{\rm arc}}{E_{\rm acc}} = \frac{P_{\rm PPT} - P_{\rm sh}}{P_{\rm PPT}} = 1 - \frac{V_{\rm sh}}{V_{\rm PPT}}$$

where the following expressions have been used:

$$P_{\rm PPT} = V_{\rm PPT} I_{\rm b}, \qquad P_{\rm sh} = V_{\rm sh} I_{\rm b}$$

Assuming that the initial condition corresponds to the maximum energy in the capacitor bank, the maximum current in the electric circuit shown in Fig. 1 is calculated by means of the following expression[13]:

$$I_{\rm b\,max} = I_{\rm b}(t_{\rm m}) = C V_0 e^{R_{\rm tot} t_m / 2L_{\rm tot}} \frac{R_{\rm tot}\cos(\omega t_m) + 2\omega L_{\rm tot}\sin(\omega {\rm t_m})}{2L_{\rm tot}}$$

where the angular frequency is

$$\omega = 2\pi / t_{\rm LRC} = 2\pi\sqrt{1/L_{\rm tot}C - (R_{\rm tot}/2L_{\rm tot})^2}$$

The maximum current occurs at the time

$$t_m = \omega^{-1}\,\text{atan}\left(\frac{4\omega^2 L_{\rm tot}^2 - R_{\rm tot}^2}{4\omega L_{\rm tot} R_{\rm tot}}\right)$$

The efficiency at the sheaths is estimated by

$$\eta_{\rm sh} = \left(1 + \frac{(V_{\rm sh})_{\rm max}}{I_{\rm max} R_{\rm PPT}}\right)^{-1} \tag{5}$$

When the current reaches its maximum value, the voltage jump at the sheaths reaches its maximum too.[5]

Arc-Generated Heat

By assumption 4 and accepting that the plasma radiates energy at constant temperature during a time $t_{\rm rad}$, the energy losses caused by heat radiation from the plasma can be expressed as

$$E_{\rm heat} = \sigma T_{\rm rad}^4 (A_{\rm rad} - A_p) t_{\rm rad} \tag{6}$$

where the action time $t_{\rm rad}$ is taken as $0.25 - 0.5\ t_{\rm LRC}$. The available energy in the arc is

$$E_{\rm arc} = \eta_{\rm trans}\eta_{\rm sh} E_0 \tag{7}$$

while the energy emitted by radiation is

$$E_{\rm rad} = \sigma T_{\rm rad}^4 A_{\rm rad} t_{\rm rad}$$

By considering that $E_{\rm arc} = E_{\rm rad} + E_{\rm em}$, it can be found that

$$T_{\rm rad} = \left(\frac{\eta_{\rm trans}\eta_{\rm sh} E_0 - E_{\rm em}}{\sigma A_{\rm rad} t_{\rm rad}}\right)^{\frac{1}{4}} \tag{8}$$

This last equation allows the writing of Eq. (6) as

$$E_{\rm heat} = (1 - \alpha_A)(\eta_{\rm trans}\eta_{\rm sh} E_0 - E_{\rm em}) \tag{9}$$

where $\alpha_A = A_p / A_{\rm rad}$ indicates the percentage of radiated energy that effectively ablates Teflon.

Energy to Ablate Teflon ($E_{\rm gas}$)

According to assumption 5, the energy $E_{\rm gas}$ is

$$E_{\rm gas} = e_{\rm gas} m \tag{10}$$

Electromagnetic Energy $E_{\rm em}$

This energy is defined as the available energy in the ionized mass and can be expressed as a function of the ionic frozen flow efficiency $\eta_{\rm fi}$. This efficiency represents the fraction of $E_{\rm em}$ that is used to increase the macroscopic velocity of the ionized mass

$$E_{\rm em} = K_{\rm em}/\eta_{\rm fi} \tag{11}$$

where $K_{\rm em}$ is the kinetic energy of the ionized ablated mass. The local enthalpy of a particle is

$$h = \int c_p\,{\rm d}T + (\varepsilon_i)_Z$$

This enthalpy includes the ionization potential to a Z level and the enthalpy of formation.

The efficiency of the ionic frozen flow will be

$$\eta_{\rm fi} = v_p^2 \big/ 2h_0$$

On the other hand, the impulse of the ion cloud with mass m_i and velocity v_i is given by

$$I_i = m_i v_i \tag{12}$$

and the electromagnetic impulse associated with the ions acceleration is[11]

$$I_{\rm em} = \frac{1}{2} L'_{\rm PPT} \int_0^T I_b^2\,{\rm d}t = \frac{L'_{\rm PPT} E_0}{2R_{\rm tot}}$$

Considering that $I_i \equiv I_{\rm em}$, the average ion velocity can be written as

$$v_i = \frac{L'_{\rm PPT} E_0}{2 m_i R_{\rm tot}}$$

Now, Eq. (11) becomes

$$E_{\rm em} = C_{\rm em}\left(E_0^2 \big/ m\right) \tag{13}$$

where

$$C_{\rm em} = (1/8\alpha_i\eta_{\rm fi})(L'_{\rm PPT}/R_{\rm tot})^2$$

Gasdynamics Energy $E_{\rm et}$

This is the energy available in the neutral ablated mass. It can be expressed as a function of the neutral frozen flow efficiency, which represents the fraction of $E_{\rm et}$ effectively used to increase the macroscopic velocity of the neutral particles

$$E_{\rm et} = K_{\rm et}/\eta_{\rm fn} \tag{14}$$

where $K_{\rm et}$ is the kinetic energy of the neutral mass. Assuming that the neutral particles travel with their maximum velocity (the velocity of sound),

$$v_p = a = \sqrt{\gamma r T}$$

then

$$\eta_{\rm fn} = \gamma r T / 2h_0$$

Thus, the kinetic energy of the neutral mass is

$$K_{\rm et} = \tfrac{1}{2} m_n V_n^2 = \tfrac{1}{2} m_n \gamma r T \tag{15}$$

By comparing Eqs. (14) and (15), it follows that

$$E_{\rm et} = m / C_{\rm et} \tag{16}$$

where

$$C_{\rm et} = \frac{2\eta_{\rm fn}}{\alpha_n \gamma r T}$$

Ablated Mass Equation

The objective of this subsection is to write Eq. (1) as a function of the ablated mass. By means of Eqs. (2), (4), (9), (10), (13), and (16), Eq. (1) can be written as

$$E_0 = (1-\eta_{\text{trans}})E_0 + (1-\eta_{\text{sh}})\eta_{\text{trans}}E_0 + (1-\alpha_A) \times (\eta_{\text{trans}}\eta_{\text{sh}}E_0 - E_{\text{em}}) + me_{\text{gas}} + C_{\text{em}}\left(E_0^2/m\right) + m/C_{\text{et}}$$

After grouping and rearrangement of terms, the preceding equation becomes

$$\left(e_{\text{gas}} + C_{\text{et}}^{-1}\right)m^2 - \alpha_A\eta_{\text{trans}}\eta_{\text{sh}}E_0 m + \alpha_A C_{\text{em}}E_0^2 = 0$$

where the solutions for the ablated mass are

$$m = \frac{\alpha_A\eta_{\text{trans}}\eta_{\text{sh}}E_0 \pm \sqrt{(\alpha_A\eta_{\text{trans}}\eta_{\text{sh}}E_0)^2 - 4\alpha_A C_{\text{em}}E_0^2\left(e_{\text{gas}} + C_{\text{et}}^{-1}\right)}}{2\left(e_{\text{gas}} + C_{\text{et}}^{-1}\right)} \tag{17}$$

This equation depends on the arc thickness δ as C_{em}, C_{et}, η_{trans}, η_{sh}, and α_A depends on it. So, to calculate the ablated mass, δ must be known.

Introduction of the Ideal Arc Thickness

To estimate the electric and geometric parameters needed for the prediction of the ablated mass, an ideal arc thickness is defined.

9) The arc has a simple geometry and is confined within the acceleration chamber.

This last assumption allows the estimation of the ohmic resistance R_{PPT}. This resistance will depend on the geometries of the acceleration chamber and the electrodes of the APPT. For instance, the resistance of the APPT shown in Fig. 1 can be approximated by

$$R_{\text{PPT}} \cong R_{\text{plasma}} = \eta_\Omega h_e/w\delta$$

Now, the total resistance of the circuit shown in Fig. 3 can be expressed as a function of the ideal arc thickness and the arc action time. Consequently, the temperature in the arc, the frozen flow efficiencies, and the sound speed are also dependent on the parameter δ.

Equations (3) and (5) show that the efficiencies η_{trans} and η_{sh} will also be dependent on the arc thickness, through the calculation of resistances R_{tot} and R_{plasma}. The ideal arc thickness determines then the maximum current occurring in the equivalent LRC circuit.

Notwithstanding the type of Teflon feeding and the electrodes geometry, it is in general possible to express the arc radiating area as a function of the Teflon exposed area, the geometry of the acceleration chamber, and the ideal arc thickness. For the APPT shown in Fig. 1, one has

$$A_{\text{rad}} = 2A_p + 2\delta(w + h_e)$$

from which α_A can be calculated.

Additionally, the determination of the ablated mass require six parameters that are not dependent on the ideal arc thickness: the inductance gradient L'_{PPT}, the total energy stored in the capacitor bank E_0, and the constants η_Ω, γ, α_i, and e_{gas}.

For several APPTs the following relation between E_{arc} and E_{em} approaches:

$$E_{\text{em}} = \tfrac{1}{2}E_{\text{arc}} \tag{18}$$

This relation, when replaced in Eq. (17), cancels the discriminant. In consequence, a unique solution to the ablated mass quadratic equation is obtained. It is

$$m = \frac{\alpha_A\eta_{\text{trans}}\eta_{\text{sh}}E_0}{2\left(e_{\text{gas}} + C_{\text{et}}^{-1}\right)} \tag{19}$$

Therefore, the ideal arc thickness δ^* calculation is based on the determination of the one that verifies Eq. (18). Given the following APPT properties—1, type of Teflon feeding; 2, Teflon exposed area; 3, geometries of the electrodes and the acceleration chamber l_e, w, h_e, e (APPT with rectangular geometry and flat electrodes) or r_{an}, r_c (APPT with coaxial geometry); 4, electric parameters C, V_0, R_{ESR}, R_{trans}, L_c, and L_{trans}; and 5, physical constants (e_{gas}, R, σ) and invariant parameters (γ, α_i, M, η_Ω)—it is possible to find δ^*.

The calculation procedure is shown in Fig. 4. However, for each APPT attention should be paid to the determination of A_p, A_{rad}, R_{plasma}, and L'_{PPT}. These values are heavily dependent on both the type of Teflon feeding and the geometry of the acceleration chamber.

Impulse Equation

Finally, the impulse is obtained by the addition of the electromagnetic and gasdynamics ones.

$$I = \frac{L'_{\text{PPT}}E_0}{2R_{\text{tot}}} + \alpha_n ma \tag{20}$$

Application of the Zero-Dimensional Analytical Model

To verify the ability of the new model for the prediction of preliminary design and performances, it is applied to five well-known APPTs: the OSU/LeRC-Benchmark PPT (Ref. 14), the LES-6 (Refs. 3, 4), the XPPT-1 (Ref. 12), the APPT given in Ref. 15 and the PPT-4 (Ref. 16). Table 1 shows the electric and geometric parameters of these five APPTs.

The first three APPTs have a two-dimensional configuration with parallel electrodes and rear-fed Teflon. The APPT given in Ref. 15 has a two-dimensional geometry, too, but Teflon is fed by means of two lateral propellant housings, and the electrodes have a 20-deg angle of divergence. The configuration of PPT-4 is coaxial and is shown in Fig. 5, where two springs laterally feed two Teflon bars among insulators of boron. These bars are pressed against the central anode, forming a cylindrical cavity that ends in a ceramic conical nozzle. The nozzle finishes in the ring cathode. Assuming that the plasma is developed geometrically as indicated in Fig. 5, the plasma resistance can be estimated as

$$R_{\text{plas}} = \eta_\Omega l_i/\pi d_m\delta$$

where l_i is the length traveled by the current in the plasma and d_m is the average diameter between d_{Teflon} and d_{an}. Approximately 30%

Table 1 Electric and geometric parameters of five APPTs

	OSU/LeRC	LES-6	XPPT-1	PPPA	PPT-4
Geometry	BF (rect.)[a]	BF (rect.)	BF (rect.)	SF (rect.)[b]	SF (coaxial)
C, μ F	10	2	10	9	8
V_0, kV	1.415	1.36	2.24	10	1.5
R_{ext}, mΩ	16	30	50	10.1	8.5
L_{ext}, nH	116	34	50	70	75
l_{an}, mm	38.1	60	100	41	l_e, mm 25
l_{cat}, mm	44.5	60	100	41	l_{cav}, mm 25
e, mm	6.4	3	5	——	d_{cav}, mm 6.4
h, mm	25.4	30	25	66	d_c, mm 4.8
w, mm	25.4	10	25	9.5[c]	d_a, mm 35.2
					$\alpha_{\text{exp.aisl}}$ 30%

[a] Breech fed.
[b] Side fed.
[c] In this case w is the distance between the two Teflon exposed surfaces. The Teflon is fed laterally. The width of the electrodes is 38 mm.

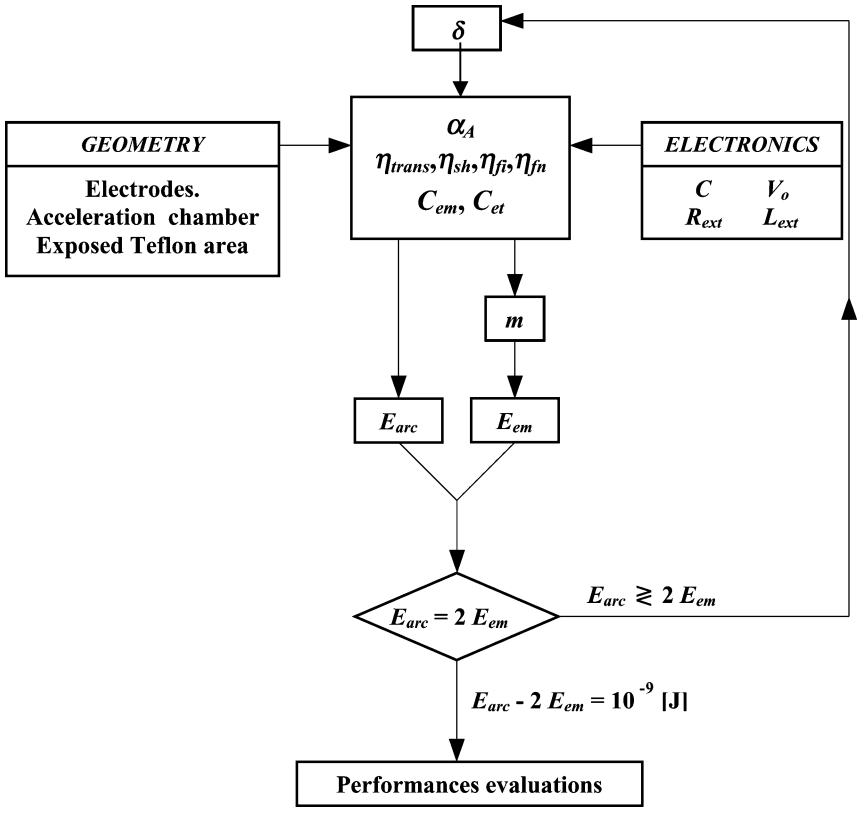

Fig. 4 Determination of the characteristic arc thickness.

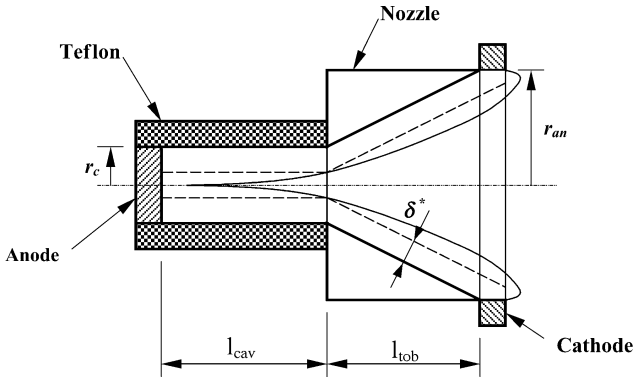

Fig. 5 Configuration of the PPT-4 module.

of the cavity inner area corresponds to the insulators, the Teflon exposed area is then given by $A_p = 0.70\pi d_{\text{cav}} l$.

For the APPTs with a two-dimensional geometry, the inductance of the system (electrodes + potential sheaths + plasma) is [17]

$$(L_{\text{PPT}})_{\text{rect}} = 0.4 l_e \left\{ \ell_n[h_e/(e+w)] + 0.22[(e+w)/l_e] - h_e/l_e + \tfrac{3}{2} \right\} \tag{21}$$

The inductance for APPTs with coaxial geometry (e.g., PPT-4) is given by

$$(L_{\text{PPT}})_{\text{coax}} = (\mu_0 l_e/2\pi)\left[\tfrac{1}{4} + \ell_n(r_a/r_c)\right]$$

The plasma resistivity can be estimated by considering a Lorentz gas and using the factor γ_E that considers the collisions electron-electron of a partially ionized gas (for $Z = 2$, $\gamma_E = 0.683$) (Ref. 18)

$$\eta_\Omega = \eta_L/\gamma_E$$

For maximum plasma temperatures around 2 eV and densities between 10^{21} m^{-3} and 10^{24} m^{-3}, the average resistivity of a doubly ionized plasma can be taken as 2×10^{-4} Ωm, which coincides with the calculations carried out in Refs. 5 and 19.

Table 2 Ionization potential and velocity for the main plasma species of the plasma

Particle	$(\varepsilon_i)_Z$, eV	Velocity, km/s	Mass × 10^{-26}, kg	Kinetic energy, eV
C	0	10 ± 5	——	6.22
C^+	11	25 ± 5	1.994	38.90
C^{++}	24	35 ± 5	——	76.24
F	0	10 ± 5	——	9.84
F^+	17	20 ± 5	3.154	39.38
F^{++}	35	30 ± 5	——	88.60

[a]Corresponds to ionization potential.[20] [b]Corresponds to velocity.[21]

The atomic mass of the gas formed by simple C and F atoms is written as

$$M = \frac{n_C M_C + n_F M_F}{n_C + n_F}$$

where M_C and M_F are the carbon and fluorine atomic mass, respectively. Although the n_C and n_F values depend on the type of APPT, their ratio can be considered as approximately constant ($n_F \cong 10$–$11 n_C$). For the PPT-4 analyzed by Keidar et al.,[5] $n_C = 0.8 \times 10^{23}\text{m} - 3$, $n_F = 9 \times 10^{23}$ m^{-3} (the maximum value being coincident with the current peak), and so the resulting mean atomic mass is $M = 18.43$ atomic mass units.

The ionization potentials, the velocity, and the kinetic energy of the main species present in the plasma are listed in Table 2. These values are useful for the determination of the ionic frozen flow efficiencies.

Results

The values of the ablated mass and the impulse bit obtained with the new model are compared with those presented in Table 3. In

Table 3 Main performances and relative error in the ablated mass *m* and the impulse bit

Performance and errors	OSU/LeRC	LES-6	XPPT-1	PPPA	PPT-4
m, μg	11.6	10	28.5	1780	45
I, μNs	——	31.2	279.5	17,000	252
m_{pred}, μg	21	2.73	23	2153	43
I_{pred}, μNs	138	21.5	155	15,700	239
e_m, %	81	72.7	19	20.9	4
e_I, %	——	31	44.5	7.9	5.2

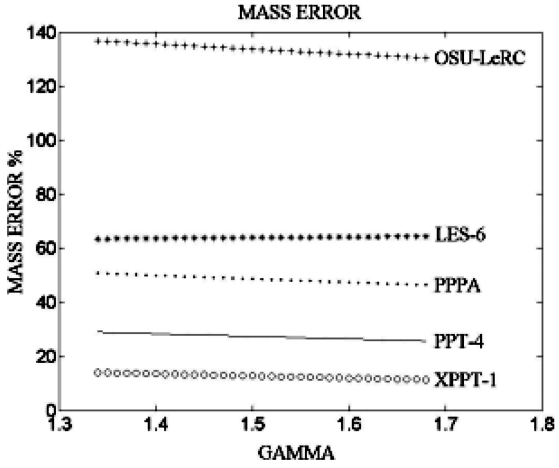

Fig. 6a Mass error for different Gamma values.

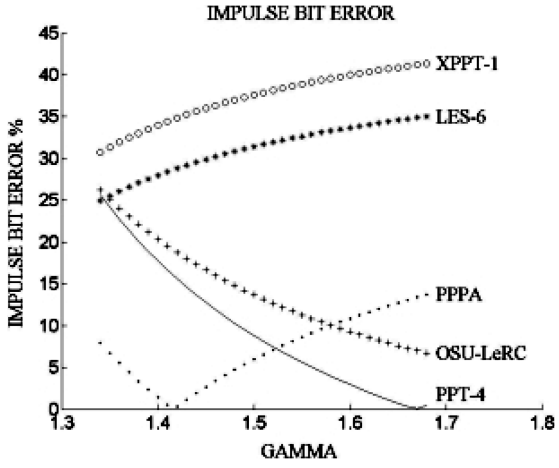

Fig. 6b Impulse bit error for different Gamma values.

all cases specific heat ratios of 1.4 have been used, and the ionized mass was assumed to be 10% of the total ablated mass. In addition, Figs. 6a and 6b represent the variation of the ablated mass and the impulse bit errors with respect to γ. These figures show that the model is practically insensitive to γ values changes.

Actually, the plasma was supposed to radiate as a blackbody because of a lack of plasma emissivities values.[11] Nevertheless, an analysis of mass error as a function of emissivities has shown that the best results are those obtained with a blackbody radiator plasma. An emissivity variation of 50% represents, in this model, a variation around 16% in mass results, and an emissivity variation of 70% increases this gap to 25%, which is not very high in comparison with the mean values of the mass relative error. The analysis of these emissivities values is based on the fact that for a Xenon plasma $0.3 < \varepsilon < 0.5$ (Ref. 22).

Comparative Analysis

The current state of the art in the development of APPTs presents relevant results and trends that can be compared to the results obtained in the present research. This comparison can be viewed as another tool for the evaluation of the capabilities and limitations of the proposed zero-dimensional model.

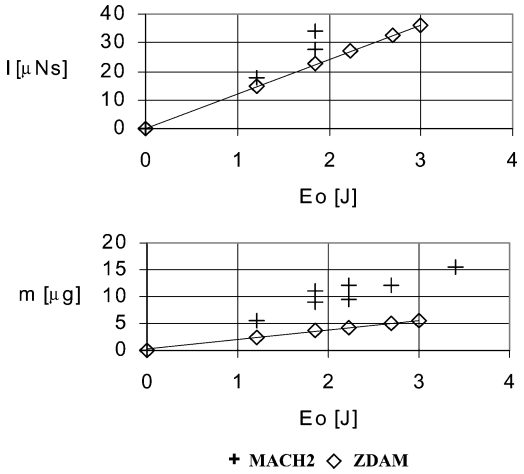

Fig. 7 Comparison between Mach 2 code results and our results for LES-6.

For the simulation of the LES-6 (two-dimensional thruster), Turchi et al.[3] use the MACH2 computational code to simulate a theoretical APPT with same dimensions as LES-6 but with coaxial geometry. The LES-6 parallel plates electrodes have a length of 6 cm and a width of 1 cm. The electrodes are separated by a gap of 3 cm. In the coaxial simulation presented in Ref. 3, the coaxial electrodes length are 6 cm, the diameter of the central cathode is 1 cm, and the diameter of the anode is 7 cm. The gap between the electrodes is thus similar to the gap between the parallel plates electrodes of LES-6. Based on the results provided by the MACH2 code,[3] it is found that

$$I_{\text{rect}}/I_{\text{coax}} \propto 1.51G(I_{\text{bmax rect}}/I_{\text{bmax coax}})^2$$

where $G = (L'_{\text{PPT}})_{\text{rect}}/(L'_{\text{PPT}})_{\text{coax}} = 7$ if $h/w = 3$ and the ratio between the anode and the cathode radii is $r_{\text{an}}/r_c = 7$. The predictions obtained with the present model yield impulse bit ratios similar to MACH2, provided E_0 is lower than 4 J.

The new model predicts a ratio between the impulse bit for rectangular geometry and the impulse bit for coaxial geometry ($I_{\text{rect}}/I_{\text{coax}}$) of approximately 2.45. This value coincides with the results published in Ref. 3.

1) Linear relationship between m, I, and E_0: The results obtained with the new model and the values calculated with MACH2 for LES-6 are compared in Fig. 7. Our results are satisfactory regarding the impulse bit, but they underestimate the ablated mass by about 50%.

2) $E_{\text{arc}}/E_{\text{em}}$ ratio: This ratio is estimated by using Eq. (11) and assuming $\eta_{\text{trans}} = 0.8$ (average value obtained by considering LES-6[11] and PPT-4[16]), $\eta_{\text{sh}} = 0.9$, and $\eta_{\text{fi}} = 0.68$ (Ref. 11).

According to Ref. 23, the ablated mass for the LES-6 is 10 μg, for a stored energy in the capacitor bank of 1.85 J, while the ions velocity is 35 km/s. The $E_{\text{arc}}/E_{\text{em}}$ ratio results approximately equal to 1.5.

For the LES-8/9, Ref. 12 gives a stored energy of 25 J and a kinetic energy of the faster ions of 4.2 J (their velocity being ~40 km/s). The corresponding energy ratio is approximately 2.7. For the XPPT-1 working with 80 J in the capacitor bank, the reported ablated mass is 106 μg, and the velocity of the ions reaches 56 km/s (Ref. 12). The energy ratio is 2.3.

Conclusions

The preliminary design of an APPT begins with the condition that the energy developed in the arc is exactly twice the electromagnetic energy applied for the ions acceleration of the plasma, consistently with the unique solution. Because of this, the accuracy of the results depends on this relation. As a result, the ablated mass and the impulse

errors are greater for those PPTs whose ratio E_{arc}/E_{em} is far from two.

Then, the design continues with the determination of the ideal arc thickness, ending with the calculation of performances. The use of this model allows the evaluation of the main performances of an APPT (impulse bit, thrust, specific impulse, propulsive efficiency, and ablated mass per pulse).

The wide spectrum of variables considered in the model permits the preliminary design of an APPT in a quite complete manner. The model is able to estimate, among others, the energy losses by heat dissipation in the circuit (including the arc) or parameters such as the average value of the temperature developed in the plasma and the maximum current developed during the discharge.

The comparison between values calculated by the model and experimental data of five APPTs yields the following mean values of the relative error: 60% for the ablated mass and 20% for the impulse bit. In spite of these rather high discrepancies between the calculated values and the experimental ones, the use of this model can be advantageous, keeping in mind that the use of empiric ablation functions leads to higher relative errors.

From the qualitative point of view of the physical representation of the phenomena involved in an APPT module, the model behaves as a reliable and robust one, because of its ability to predict trends and behaviors that have been previously verified through experimental work.

Contrary to the empiric functions of ablation, the model bears some additional advantages. First, it allows for sensitivity studies involving performance parameters, and second, improved submodels or the theoretical simulation of different combinations of electric-geometric parameters can also be integrated into the model.

The possibility of being able to assess the influence of the geometry, the electronics, the atomic nature of the plasma and neutral particles on the energy balance in the whole APPT offers a road toward the elaboration of more complete models. This fact, in addition to the possibility of conceptually understanding APPTs behaviors, should be considered as a balancing factor against the analytical (zero-dimensional) approximation drawbacks.

Acknowledgments

This work has been supported by means of Grants PICT-99-10-07107 of Argentina's National Agency for the support of Science and Technology, "Theoretical and Numerical Studies and Applications of the Plasmas and Gases Dynamics" of National University of Cordoba, and "A Theoretical-Experimental Study of the Pulsed Plasma Thruster" of Cordoba Science Agency. A fellowship granted by the National University of Cordoba has made possible the fourth author participation in this project.

References

[1]Myers, R. M., and Cassady, R. J., "Overview of Major U.S. Industrial Programs in Electric Propulsion," AIAA Paper 98-3179, July 1998.

[2]Rayburn, C., Campbell, M., Hoskins, W., and Cassady, R., "Development of a Micro Pulsed Plasma Thruster for the Dawgstar Nanosatellite," AIAA Paper 2000-3256, July 2000.

[3]Turchi, P. J., Mikellides, I. G., Mikellides, P. G., and Schmahl, C. S., "Theoretical Investigation of Pulsed Plasma Thrusters," AIAA Paper 98-3807, July 1998.

[4]Mikellides, P. G., and Turchi, P. J., "Modeling of Late-Time Ablation in Pulsed Plasma Thrusters," AIAA Paper 96-2733, July 1996.

[5]Keidar, M., Boyd, I. D., and Beilis, I. I., "A Model of an Electrical Discharge in a Coaxial Pulsed Plasma Thruster," International Electric Propulsion Conference, Paper 99-214, Oct. 1999.

[6]Guman, W. J., "Designing Solid Propellant Pulsed Plasma Thrusters," AIAA Paper 75-410, March 1975.

[7]Rudikov, A. I., Antropov, N. N., and Popov, G. A., "Pulsed Plasma Thruster of Erosion Type for a Geostationary Artificial Earth Satellite," International Astronautical Federation, Paper 93-S.5.487, Oct. 1993.

[8]Ziemer, J. K., Choueiri, E. Y., and Jahn, R. G., "Scaling Laws for Pulsed Electric Propulsion with Application to the Pluto Express Mission," *Proceedings of the 24th International Electric Propulsion Conference*, Paper IEPC-95-147, Electric Propulsion and Plasma Dynamics Lab., Princeton Univ., NJ, 1995.

[9]Chen, Z., and Brandhorst, H., "Performance of High Power Capacitors for Pulsed Plasma Thruster Applications," International Electric Propulsion Conference, Paper 99-060, Oct. 1999.

[10]Vondra, R. J., and Thomassen, K., "Flight Qualified Pulsed Electric Thruster for Satellite Control," *Journal of Spacecraft and Rockets*, Vol. 11, No. 9, 1974, pp. 613–617.

[11]Burton, R. L., Wilson, M. J., and Bushman, S. S., "Energy Balance and Efficiency of the Pulsed Plasma Thruster," AIAA Paper 98-3808, July 1998.

[12]Spanjers, G. G., McFall, K. A., Gulczinski, F. S., and Spores, R. A., "Investigation of Propellant Inefficiencies in a Pulsed Plasma Thruster," AIAA Paper 96-2723, July 1996.

[13]Halliday, D., and Resnick, R., *Physics for Students of Science and Engineering*, 2nd ed., Pt. 2, Wiley, New York, 1962, pp. 858, 859.

[14]Kamhawi, H., Turchi, P. J., Leiweke, R. J., and Myers, R. M., "Design and Operation of a Laboratory Benchmark PPT," AIAA Paper 96-2732, July 1996.

[15]Palumbo, D. J., and Guman, W. J., "Effects of Propellant and Electrode Geometry on Pulsed Ablative Plasma Thruster Performance," AIAA Paper 75-409, March 1975.

[16]Bushman, S. S., Burton, R. L., and Antonsen, E. L., "Arc Measurements and Performance Characteristics of a Coaxial Pulsed Plasma Thruster," AIAA Paper 98-3660, July 1998.

[17]Anderson, H. L. (ed.), *Physics Vade Mecum*, American Inst. of Physics, New York, 1981.

[18]Spitzer, L., Jr., *Physique des Gaz Completement Ionisés*, Monographies Dunod, Dunod, Paris, 1959, pp. 91–95.

[19]Eckman, R., Byrne, L., Cameron, E., Gatsonis, N. A., and Pencil, E., "Triple Langmuir Probe Measurements in the Plume of a Pulsed Plasma Thruster," *Journal of Propulsion and Power*, Vol. 17, No. 4, 2001, pp. 762–771.

[20]Fano, U., and Fano, L., *Basic Physics of Atoms and Molecules*, Wiley, New York, 1959, p. 45.

[21]Thomassen, K. L., and Vondra, R. J., "Exhaust Velocity Studies of a Solid Teflón Pulsed Plasma Thruster," *Journal of Spacecraft and Rockets*, Vol. 9, No. 1, 1972, pp. 61–64.

[22]Church, C. H., Schlecht, R. G., Liberman, I., and Swanson, B. W., "Studies of Highly Radiative Plasma Using the Wall-Stabilized Pulsed Arc Discharge," *AIAA Journal*, Vol. 4, No. 11, 1966, pp. 1947–1953.

[23]Mikellides, I. G., and Turchi, P. J., "Optimization of Pulsed Plasma Thrusters in Rectangular and Coaxial Geometries," International Electric Propulsion Conference, Paper 99-211, Oct. 1999.